View metadata, citation and similar papers at core.ac.uk

brought to you by CORE

provided by CiteSeerX

An Investigation of Thin-Film Coating/Substrate Systems by Nanoindentation

Jackie Li

Erik T. Thostenson

Tsu-Wei Chou

Center for Composite Materials, and Department of Mechanical Engineering, University of Delaware, Newark, DE 19716

Laura Riester

MS 6069, P. O. Box 2008, Oak Ridge National Laboratory, Oak Ridge, TN 37831-6069

The indentation load-displacement behavior of three material systems tested with a Berkovich indenter has been examined. The materials studied were the substrate materials—silicon and polycarbonate, and the coating/substrate systems—diamond-like carbon (DLC) coating on silicon, and DLC coating on polycarbonate. They represent three material systems, namely, bulk, soft-coating on hard-substrate, and hard-coating on soft-substrate. Delaminations in the soft-coating/hard-substrate (DLC/Si) system and cracking in the hard-coating/soft-substrate system (DLC/Polycarbonate) were observed. Parallel to the experimental work, an elastic analytical effort has been made to examine the influence of the film thickness and the properties of the coating/substrate systems. Comparisons between the experimental data and analytical solutions of the load-displacement curves during unloading show good agreement. The analytical solution also suggests that the Young's modulus and hardness of the thin film can not be measured accurately using Sneddon's solution for bulk materials when the thickness of the film is comparable to the loading contact radius of the indenter. The elastic stress field analysis provides a basis for understanding the experimentally observed delaminations and cracking of the coating/substrate systems.

1 Introduction

Thin-film techniques have been extensively used in industry. With the development of applications of thin-film coating materials, measurement of the adherence and mechanical behavior of the coating/substrate systems have received considerable attention. For instance, among the others, Marshall et al. (1984) and Rossington et al. (1984) have measured the adherence of thin films due to residual stresses by indentation. Mattewson (1986) has also studied the adhesion measurement of thin films by indentation. Evans and Hutchinson (1984) have studied delamination and spalling in compressed films. Doerner and Nix (1986) provided a method for interpreting the data from depth-sensing indentation instruments. Stone et al. (1988) have investigated the hardness and adhesion of sputter-deposited aluminum on silicon by utilizing a continuous indentation test. Van der Zwaag et al. (1986), and Lardner et al. (1992) have studied the effect of double layer coatings on contact stresses.

In this paper, first, nanoindentation tests have been carried out for bulk, soft-coating/substrate and hard-coating/substrate systems. The experiments provide the load-displacement curves which can be used to obtain the elastic properties of the system. The failure phenomena such as delamination and cracking of the thin-film coating/substrate systems have also been observed. Next, we applied a theoretical model of the coating/substrate system developed by Li and Chou (1997) to compare with the experimental results. This newly developed analysis can account for the influences of the elastic properties of both the film and substrate, as well as the film thickness. Unlike most existing works for which numerical iterations (see Chiu and Hartnett, 1983, and O'Sullivan and King, 1988) and finite element analysis (i.e, Van der Zwaag and Field, 1982; Komvopoulos, et al., 1987, 1995(a, b), and Jayachandran, et al., 1995) have been used, the solutions here are capable of capturing the essential features of the indentation of thin-film coating/substrate systems in the elastic range. The comparisons between experimental data and theoretical modeling for the load-indentation depth curves are made and shown a good agreement to each other. The elastic stress field obtained from the analytical solutions can be used to explain the experimentally observed failure mechanisms of coating/substrate systems.

2 Experimental

Diamond-like carbon (DLC) thin-film material was used for the experimental investigation, which was deposited through ion beam deposition. To examine the influence of the substrate elastic properties on the mechanical behavior of the thin-film/substrate systems, the DLC coating was applied to silicon (hard substrate) and polycarbonate (soft substrate). In the soft-coating/substrate system (DLC/silicon), the film thickness was varied to examine its influence.

The mechanical properties of the thin-film/substrate systems were characterized by using a Nanoindenter II® (Nano Instruments, Inc., Knoxville, TN) Mechanical Properties Microprobe at the High Temperature Materials Laboratory of the Oak Ridge National Laboratory. Each specimen was tested using the continuous stiffness measurement technique developed by Oliver and Pethica (1989). This technique enables continuous measurement of the stiffness and area of contact between the indenter and the specimen during indentation. The contact stiffness, applied load and indenter displacement can then be used to determine the mechanical properties such as Young's modulus and hardness. This technique allows for measurement of the mechanical properties as a function of the indentation depth and can be used to examine the effect of the substrate on the mechanical properties of the film.

The indentation experiments were performed at room temperature with a diamond Berkovich (three-sided pyramid) indenter tip. For the DLC/silicon system, specimens were tested with film thicknesses of 2 μm and 0.1 μm. In addition, uncoated silicon was tested to determine the mechanical properties of the substrate. The thickness of the DLC on polycarbonate was 0.1 μm, and the DLC/polycarbonate system has an interlayer of polysiloxane to improve adhesion between the film and sub-

Contributed by the Materials Division for publication in the JOURNAL OF ENGINEERING MATERIALS AND TECHNOLOGY. Manuscript received by the Materials Division June 30, 1997; revised manuscript received November 17, 1997. Associate Technical Editor: G. J. Weng.

Copyright © 1998 by ASME

Downloaded From: https://materialstechnology.asmedigitalcollection.asme.org on 07/02/2019 Terms of Use: http://www.asme.org/about-asme/terms-of-use

strate. Specimens of the polycarbonate treated with polysiloxane were tested with and without the DLC thin film. On each of the specimens, five indentations were performed at different depths: 4 μm, 2 μm, 800 nm, 200 nm, and 40 nm. Areas where the specimens were indented were selected by viewing the sample surface under the optical microscope prior to indentation (Fig. 1).

3 Experimental Results

3.1 Load-Displacement Curves. The experimental load-displacement curves for uncoated substrates of Si and polycarbonate, and the coated systems of DLC/Si and DLC/polycarbonate were obtained. Figures 2–5 present typical indentation load-displacement curves in a load-unloading cycle for the material systems under the peak loads around 660 mN for Si, 22 mN for polycarbonate, 160 mN for DLC/Si, and 20 mN for DLC/polycarbonate. The displacement (d) at unloading and the final displacement (d_f) are indicated in Fig. 4. All four material systems exhibit plastic deformation after unloading. Since the stiffness of DLC/Si is much higher than that of DLC/polycarbonate, the depth of indentation on DLC/polycarbonate shown in Fig. 5 reaches 2 μm at the peak load around 20 mN, while the depth of the DLC/Si system shown in Fig. 4 is only around 0.9 μm at the peak load of 160 mN. The bulk silicon (Fig. 2) is stiffer then the DLC and thus shows less indentation depth then the DLC/Si system at the same magnitude of loads.

3.2 Young's Modulus. Using the load-indentation depth curves and the continuous stiffness measurement method suggested by Oliver and Pethica (1989), the Young's modulus of the coating/substrate systems can be obtained. Figures 6–9 show the Young's moduli for silicon, polycarbonate, DLC/Si, and DLC/polycarbonate systems, respectively.

The Young's modulus data of Si shown in Fig. 6 remain nearly constant over the range of indentation depth measured. This result is expected for the bulk material, and the approximate average value of Young's modulus is 180 GPa. Similarly, the Young's modulus value of 3.3 GPa for polycarbonate can be obtained approximately from Fig. 7. When DLC is deposited on the Si substrate with the coating thickness of 2 μm, the elastic modulus of the coating/substrate system shown in Fig. 8 is no longer constant. As the indentation depth increases, the modulus also increases, gradually approaching that of the bulk Si substrate (180 GPa), at which the indentation depth (2 μm) reaches the coating/substrate interface. The result of Fig. 8 indicates that the DLC material is elastically less stiff than the Si substrate. The effect of the substrate can be observed at penetration depths $d > 10\%$ of the film thickness (see Oliver et al., 1989). To further quantify the effect of the substrate, we enlarged the horizontal scale and replotted the data of initial displacement, and inserted the results in Fig. 8. From this, the Young's modulus of DLC coating then can be estimated as

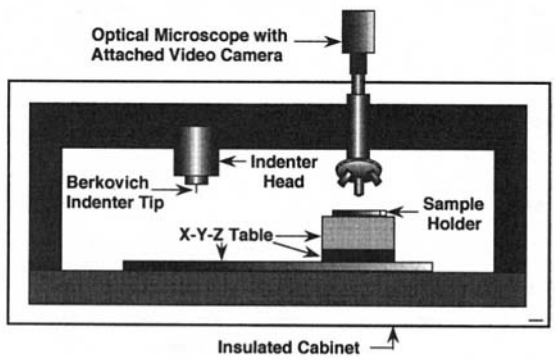

Fig. 1 A schematic diagram of experimental set-up of nanoindentation

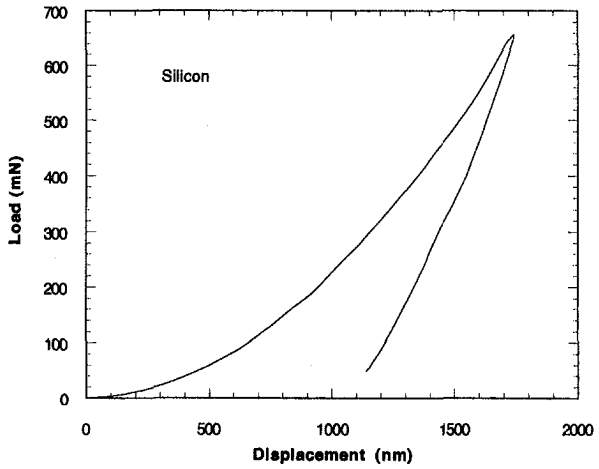

Fig. 2 Load-indentation displacement curve of silicon bulk material under nanoindentation with the maximum load of 660 mN

130 GPa. Figure 9 shows the elastic modulus of the DLC/polycarbonate system with the DLC thickness of 0.1 μm. Since the DLC coating material is much stiffer than the polycarbonate substrate, the elastic modulus decreases sharply at the early stage of indentation and reaches the saturation value of 3.3 GPa when the indenter penetrates deeper into the polycarbonate substrate.

3.3 Observations of Failures. Figure 10 is a micrograph of the Si bulk material with the indentation depths of 4 μm, 2 μm and 800 nm. Little damage around the indentation site has been observed even though there is a bubble observed near one of the contact edges for the 4 μm depth indentation.

Figures 11(a) and (b) show the micrographs of the DLC/Si system at the indentation depth of 2 μm. In Fig. 11(a) the DLC thickness is about 2 μm, and the perfect pyramid shape of the indent indicates that there is little damage. However, for the case of 0.1 μm thickness of DLC on Si substrate shown in Fig. 11(b), debonding between the coating film and substrate around the contact edge can be observed clearly. This is a common phenomenon for the soft-coating/hard-substrate system, which has been reported by other researchers (for example, Ritter et al. (1989) observed the debonding of epoxy coating on glass under a spherical indentation).

Figure 12 is a micrograph showing cracks in DLC/polycarbonate with the coating thickness of 0.1 μm. The indentation depth is around 4 μm. Instead of delamination, cracking of the film along the three edges of the indenter and circumferential cracks in the triangular contact zone occur first in this hard-coating/soft-substrate system.

The physical reasons for the different damage modes of soft-coating and hard-coating/substrate systems will be further discussed after the theoretical modeling is introduced in Section IV.

4 Theoretical Modeling

In this section, we recapitulate the results of a recent theoretical study by Li and Chou (1997) on nanoindentation of coating/substrate systems. First, it should be mentioned that Gao and Wu (1993) have shown that an axisymmetric flat-ended cylindrical punch can be used to model nonaxisymmetric indentations using, for example, Vickers and Berkovich indenters, since the elastic contact stiffness is insensitive to the cross-section shape of the indenter as long as the shape does not differ too much from a circle. Li and Chou (1997) developed the elastic solution of the coating/substrate systems under an axisymmetric loading to model the problem of nanoindentation using Berkov-

Downloaded From: https://materialstechnology.asmedigitalcollection.asme.org on 07/02/2019 Terms of Use: http://www.asme.org/about-asme/terms-of-use

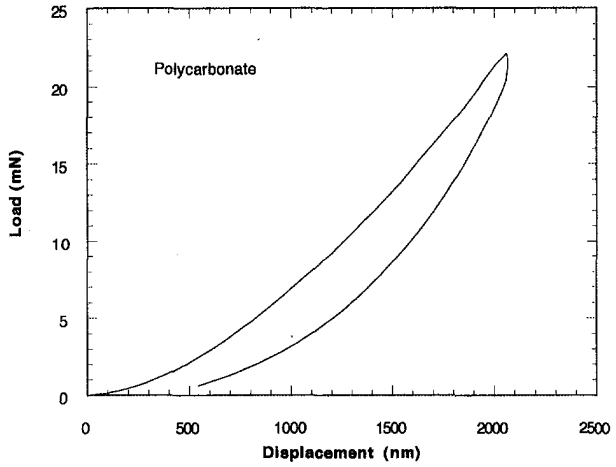

Fig. 3 Load-indentation displacement curve of polycarbonate under nanoindentation

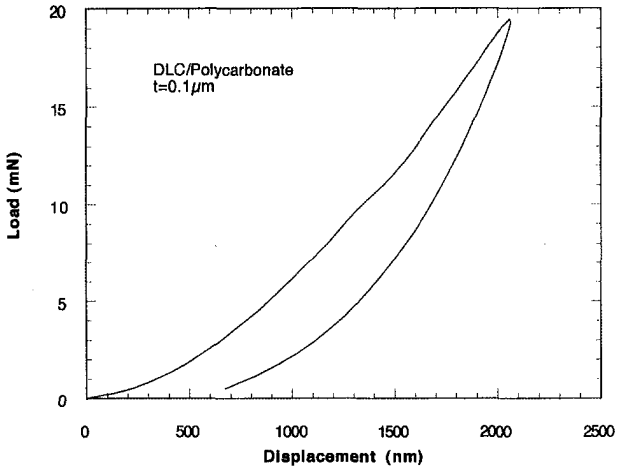

Fig. 5 Load-indentation displacement curve of DLC/polycarbonate under nanoindentation with the maximum load of 60 mN

ich indenter. Here we briefly outline this analytic method, as the details can be found in Li and Chou (1997).

A schematic of the geometry of the problem is shown in Fig. 13. The thin-film coating is referred to as phase 1 and the substrate as phase 0. For simplicity, both phases are assumed to be isotropic, with Young's modulus and Poisson's ratio denoted by E_r and ν_r, respectively, for the rth phase; the shear modulus is $\mu_r = E_r/(2(1 + \nu_r))$. The thickness of the film is denoted as t. An arbitrary normal distributed stress with the loading contact radius r_o is applied on the free surface symmetrically with respect to the z-axis. Here we use the cylindrical polar coordinates (r, θ, z) and denote the displacements as u, v and w along the r-, θ-, and z-directions, respectively. The stress components are denoted as σ_r, σ_θ, σ_z, $\tau_{r\theta}$, $\tau_{\theta z}$, and τ_{zr}.

The symmetry condition with respect to the z-axis implies that v, $\tau_{r\theta}$ and $\tau_{\theta z}$ all vanish, and the equilibrium equations are reduced to

$$\frac{\partial \sigma_r}{\partial r} + \frac{\partial \tau_{rz}}{\partial z} + \frac{1}{r}(\sigma_r - \sigma_\theta) = 0 \tag{1}$$

$$\frac{\partial \tau_{rz}}{\partial r} + \frac{\partial \sigma_z}{\partial z} + \frac{\tau_{zr}}{r} = 0. \tag{2}$$

By introducing a stress function Φ, the stress components and displacements can be expressed in terms of Φ as follows:

$$\sigma_r = \lambda \nabla^2 \Phi_z - 2(\lambda + \mu)\Phi_{rrz}$$

$$\sigma_z = (3\lambda + 4\mu)\nabla^2 \Phi_z - 2(\lambda + \mu)\Phi_{zzz}$$

$$\sigma_\theta = \lambda \nabla^2 \Phi_z - 2(\lambda + \mu)\frac{1}{r}\Phi_{rz}$$

$$\tau_{zr} = (\lambda + 2\mu)\frac{\partial}{\partial r}\nabla^2 \Phi - 2(\lambda + \mu)\Phi_{zzr} \tag{3}$$

and

$$u_r = -\frac{\lambda + \mu}{\lambda}\Phi_{rz}$$

$$u_z = \frac{\lambda + 2\mu}{\mu}\nabla^2 \Phi - \frac{\lambda + \mu}{\mu}\Phi_{zz} \tag{4}$$

where λ is the Láme constant, and $\Phi_{rrz} = \partial^3\Phi/\partial r^2 \partial z$. In the case of axial symmetry, $\nabla^2 \equiv (\partial^2/\partial r^2) + (1/r)(\partial/\partial r) + (\partial^2/\partial z^2)$. Then the compatibility equation can be written as

$$\nabla^4 \Phi = 0. \tag{5}$$

Following Harding and Sneddon (1945) the Hankel's transform is applied to solve the above biharmonic equation

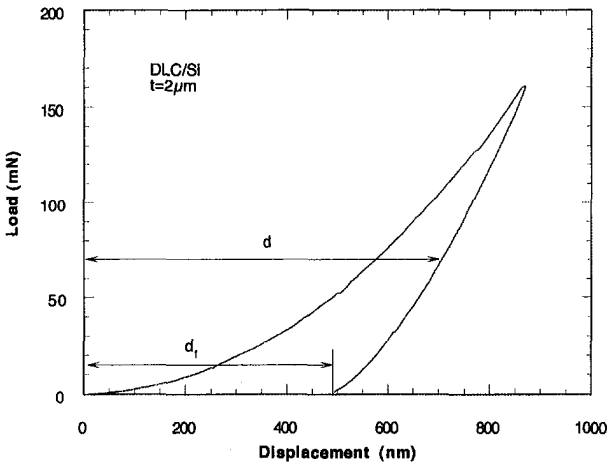

Fig. 4 Load-indentation displacement curve of DLC/Si system under nanoindentation with the maximum load of 160 mN

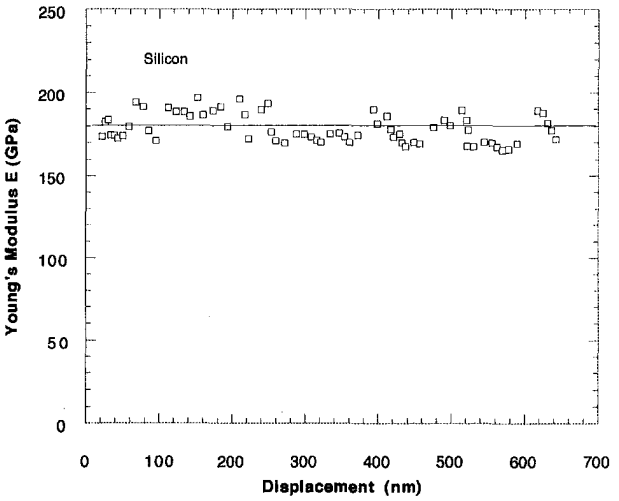

Fig. 6 Young's modulus versus indentation displacement of silicon

Downloaded From: https://materialstechnology.asmedigitalcollection.asme.org on 07/02/2019 Terms of Use: http://www.asme.org/about-asme/terms-of-use

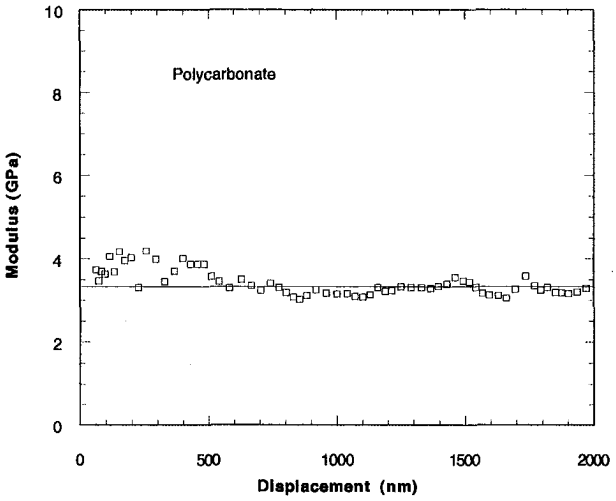

Fig. 7 Young's modulus versus indentation displacement of polycarbonate

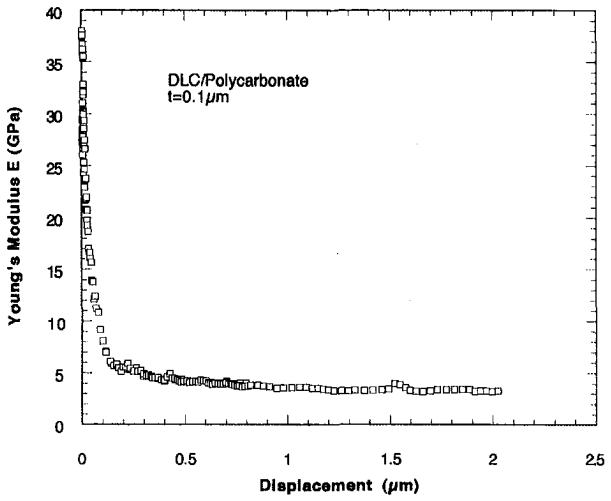

Fig. 9 Young's modulus versus indentation displacement of DLC/polycarbonate

$$G = \int_0^\infty \Phi r J_0(\xi r) dr \tag{6}$$

where $J_0(\xi r)$ is a Bessel function of the first kind of order 0. Thus, Eq. (5) is reduced to an ordinary differential equation

$$\left(\frac{d^2}{dz^2} - \xi^2\right)^2 G = 0. \tag{7}$$

The solution of Eq. (7) is easily obtained as

$$G = (A + Bz)e^{\xi z} + (C + Dz)e^{-\xi z} \tag{8}$$

where A, B, C, and D are constants which are in general functions of ξ and can be determined from the boundary conditions. By inverting Hankel's transform, the stress function can be solved as

$$\Phi = \int_0^\infty \xi G J_0(\xi r) d\xi. \tag{9}$$

Based upon Eq. (9), the stress and displacement fields can be obtained from Eqs. (3) and (4).

For the material systems considered here, the stress function Φ needs to be found for the coating as well as for the substrate. Thus, instead of four coefficients in Eq. (8) there are eight coefficients denoted as A_0, B_0, C_0, D_0, A_1, B_1, C_1, and D_1, where the subscripts 0 and 1 represent the substrate and coating phase, respectively. Since all the stresses and displacements vanish when $z \to \infty$, A_0 and B_0 must be zero, and the remaining six coefficients can be determined from the boundary and interfacial continuity conditions.

The boundary loading conditions in the indentation problem considered here are expressed as

$$\sigma_z(r, 0) = -q(r), \quad \tau_{zr}(r, 0) = 0 \tag{10}$$

where the negative sign in the first equation represents a compression, and the function $q(r)$ can be further expressed in terms of Hankel's transform as

$$q(r) = \int_0^\infty \bar{q}(\xi)\xi J_0(\xi r) d\xi. \tag{11}$$

Perfect bonding at the interface between the film and the substrate is assumed. Then the interfacial continuity conditions at the plane $z = t$ are given as

$$u_1(r, t) = u_0(r, t) \quad w_1(r, t) = w_0(r, t)$$
$$\sigma_{z1}(r, t) = \sigma_{z0}(r, t) \quad \tau_{zr1}(r, t) = \tau_{zr0}(r, t) \tag{12}$$

For the coating/substrate system, the stress distribution on the loading surface is unknown, and it is difficult to determine from the displacement profile. Thus, in order to simulate the non-

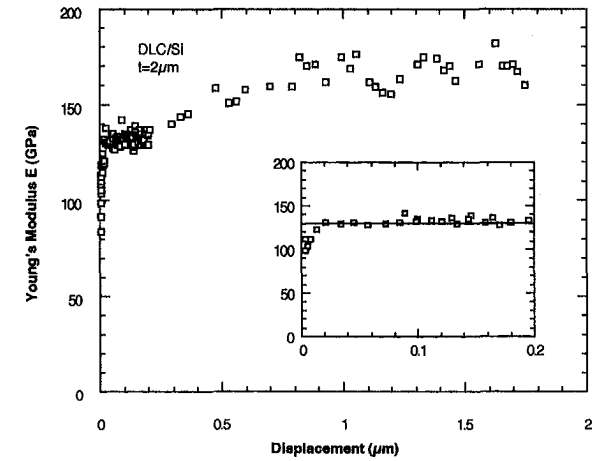

Fig. 8 Young's modulus versus indentation displacement of DLC/Si

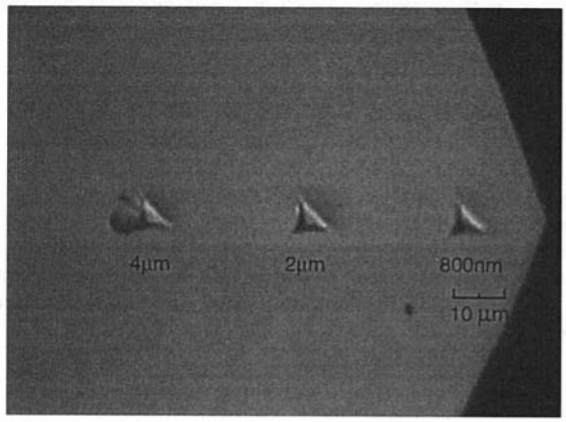

Fig. 10 Micrograph of 4 μm, 2 μm and 800 nm indentations in silicon

Downloaded From: https://materialstechnology.asmedigitalcollection.asme.org on 07/02/2019 Terms of Use: http://www.asme.org/about-asme/terms-of-use

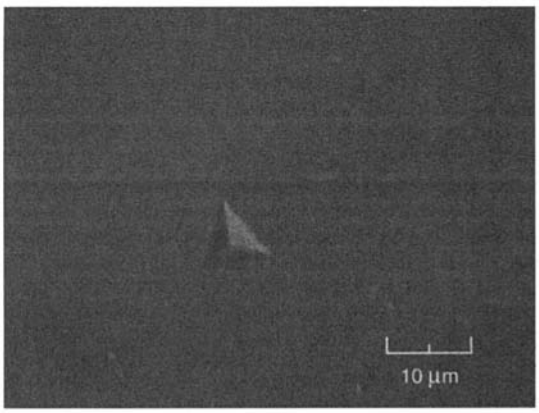

(a)

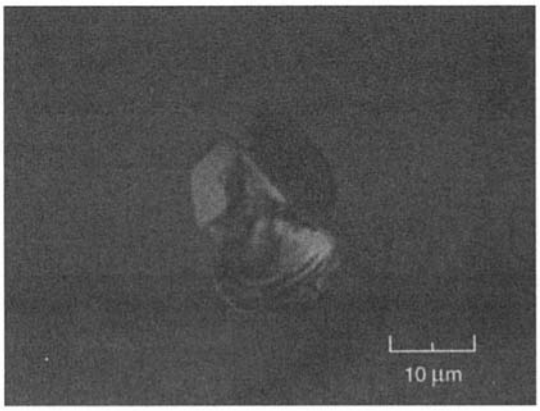

(b)

Fig. 11 Micrographs of 2 μm indentation in DLC/Si system with (*a*) 2 μm thickness of DLC, and (*b*) 0.1 μm thickness of DLC

uniform loading distribution of the indentation problem, the following form of surface loading is assumed:

$$q(r) = \begin{cases} \sigma_m \left[1 - \left(\frac{r}{r_0} \right)^2 \right] & r \le r_0 \\ 0 & r > r_0 \end{cases} \tag{13}$$

where σ_m is the maximum stress at $r = 0$, and r_0 is the loading contact radius. Then $q(r)$ in Hankel's transform domain, $\bar{q}(\xi)$, can be written as

$$\bar{q}(\xi) = 2 \frac{\sigma_m t^2}{\rho_0} \left[\frac{2}{\eta^3} J_1(\rho_0 \eta) - \frac{\rho_0}{\eta^2} J_0(\rho_0 \eta) \right] \tag{14}$$

where $\rho_0 = r_0/t$ and $\eta = \xi t$. Then the components of stress and displacement can be solved accordingly.

Next, the relation between the total applied load and the indentation depth needs to be determined. For the loading condition given in Eq. (13), the total normal force on the surface is obtained as

$$P = 2\pi \int_0^{r_0} r q(r) dr = \frac{\pi}{2} \sigma_m r_0^2. \tag{15}$$

It should be noted that the maximum stress σ_m is not constant when the total indentation force P changes. Here we further assume that the maximum stress σ_m is proportional to the loading contact radius r_0 as

$$\sigma_m = \sigma_0 \frac{r_0}{t} \tag{16}$$

where σ_0 is a constant reference stress and t is the thickness of the film as a reference length. The assumption given in Eq. (16) was motivated by the exact solution for a homogeneous half-space under a rigid spherical indentation given by Harding and Sneddon (1945) where the applied load P is proportional to r_0^3. Substituting Eq. (16) into Eq. (15), the total load can be rewritten as

$$P = \frac{t^2 \pi \sigma_0}{2} \rho_0^3. \tag{17}$$

Then the penetration depth, $d = w(0, 0)$, of the indenter (in this work, the elastic displacement during unloading is given by $d - d_f$) is obtained

$$\frac{\mu_0}{2\sigma_0} \frac{d - d_f}{t} = \int_0^\infty \left[\frac{2}{\eta^3} J_1(\rho_0 \eta) - \frac{\rho_0}{\eta^2} J_0(\rho_0 \eta) \right] \times \frac{1 + 4b\eta e^{-2\eta} - abe^{-4\eta}}{\alpha D(\eta)} d\eta \tag{18}$$

where

$$a = \frac{(3 - 4\nu_0)\alpha - (3 - 4\nu_1)}{1 + (3 - 4\nu_0)\alpha}, \quad b = \frac{\alpha - 1}{\alpha + (3 - 4\nu_1)}, \quad \alpha = \frac{\mu_1}{\mu_0} \tag{19}$$

and

$$D(\eta) = 1 - (a + b + 4b\eta^2)e^{-2\eta} + abe^{-4\eta}. \tag{20}$$

Equations (17) and (18) give the relationship of the total indentation load P and the indentation depth d, and it can be used to compare with the experimental data.

5 Comparison of Experimental Data and Analytical Solution

In this section the theoretical analysis is applied to the coating/substrate systems tested by Berkovich nanoindentation. Parallel to section III, there are three parts as follows:

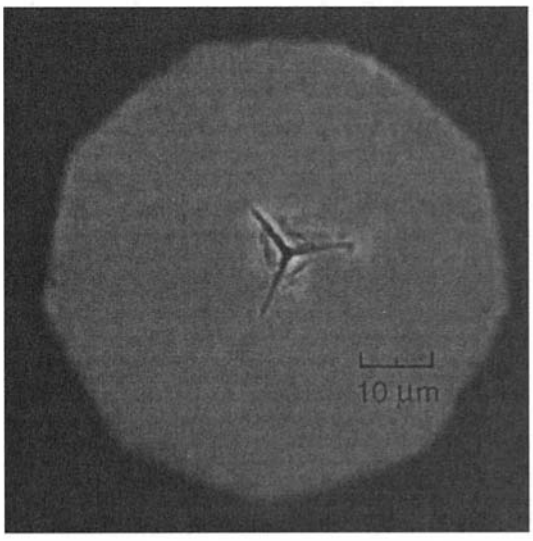

Fig. 12 Micrograph of 4 μm indentation in DLC/polycarbonate system

Downloaded From: https://materialstechnology.asmedigitalcollection.asme.org on 07/02/2019 Terms of Use: http://www.asme.org/about-asme/terms-of-use

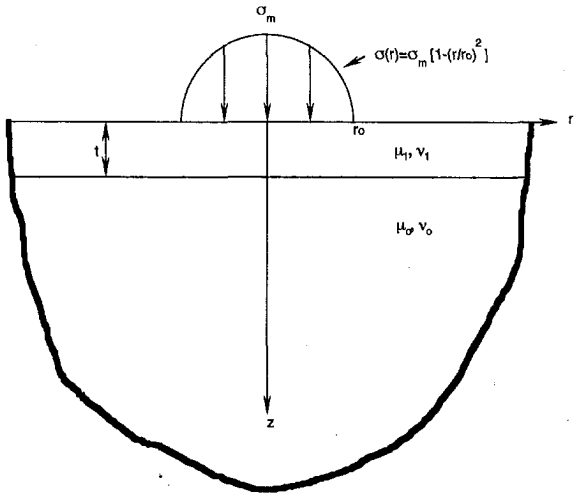

Fig. 13 A schematic diagram of a coating/substrate system under axisymmetrical loading

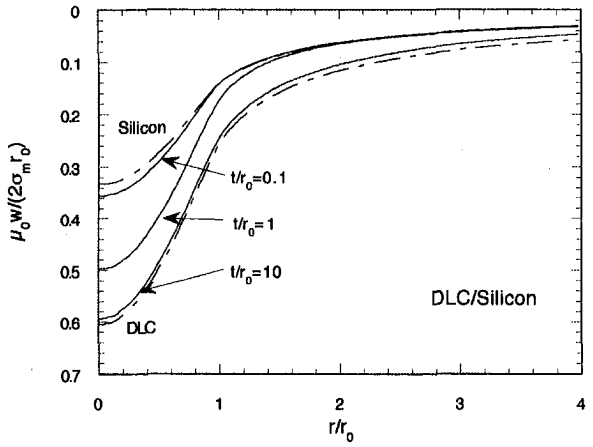

Fig. 15 Influence of DLC coating thickness on surface displacement profiles of DLC/Si system

5.1 Comparison of Load-Displacement Relations. It can be seen from the indentation load-depth curves of Figs. 2–5 that plastic deformation developed in all three material systems: bulk Si and polycarbonate, DLC/Si, and DLC/polycarbonate. Since the analytical model is based upon elastic deformation, and the unloading curves have been observed by other researchers (for example, Doerner and Nix, 1986) to involve essentially elastic deformation, the unloading curves have been used here to compare with theoretical predictions.

First, by fitting the theoretical result given by Eq. (18) to the experimental load-displacement data (solid circles in Fig. 14) of the bulk silicon during unloading, the constant reference stress σ_0 = 7.2 GPa in Eq. (17) is obtained. The Young's modulus of silicon has been found to be E_0 = 180 GPa approximately from the experimental data shown in Fig. 6, and the Poisson's ratio is assumed to be ν_0 = 0.2. Here, d and d_f are defined in Fig. 4.

For the DLC/Si coating/substrate system, the Young's modulus of the DLC can be approximately obtained from Fig. 8 as E_1 = 130 GPa, and the Poisson's ratio is also assumed to be ν_1 = 0.2. Using the σ_0 value obtained above, the analytical solution of the indentation load-depth curve of the DLC/Si system with the film thickness 2 μm calculated from Eq. (18) is given by the lower solid line in Fig. 14. The motivation for developing the analytical curve is explained below. Experimental results have shown that delamination occured in the DLC/Si system with 0.1 μm film thickness when the indentation depth reached 2 μm (see Fig. 11(b)), but not for the DLC/Si system with 2 μm film thickness. The unloading curve of Fig. 4 shows that the maximum indentation depth is less than 1 μm. This implies that delamination has not occured yet in this coating/substrate system, and only plastic deformation has developed during the loading process. Thus, it can be concluded that the unloading curve is essentially due to elastic deformation. The agreement between the experimental data (solid triangles) and the theoretical prediction is quite good.

The comparison between theory and experiments explained above is not applicable to polycarbonate and DLC/polycarbonate of which the load-depth curves are shown in Figs. 3 and 5. This is because that polycarbonate is a viscoelastic material, and cracking in the DLC/polycarbonate system with 0.1 μm film thickness may have already occurred.

5.2 Influence of the Film Thickness. The displacement profiles on the coating surface of DLC/Si and DLC/polycarbonate systems are shown in Figs. 15 and 16, respectively. The derivation of the elastic field can be found in Li and Chou (1997). The displacement and stress components are recapitulated in the Appendix. The figures show that the surface displacement profiles of the coating/substrate systems always lie in between those of the film and the substrate materials. For the soft-coating/hard-substrate combination such as the DLC/Si system shown in Fig. 15, the substrate gives the lower bound of displacement, while the film gives the upper bound. The

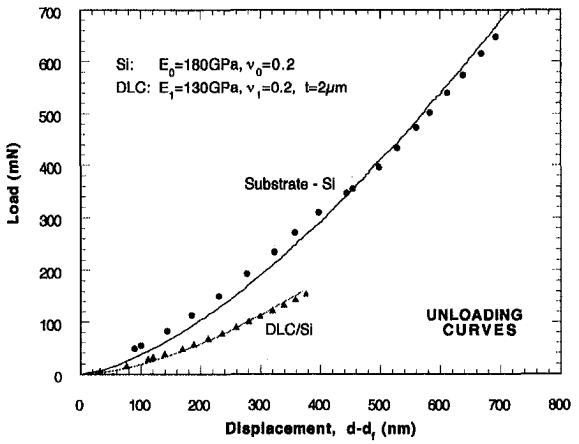

Fig. 14 Comparison of load-indentation displacement curves between the experimental data and theoretical modeling for both silicon and DLC/Si systems during unloading

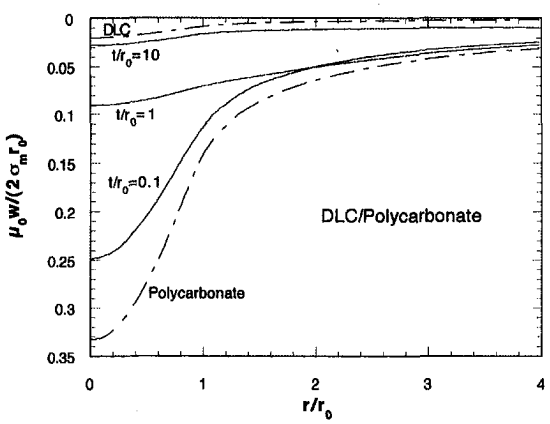

Fig. 16 Influence of DLC coating thickness on surface displacement profiles of DLC/polycarbonate system

Downloaded From: https://materialstechnology.asmedigitalcollection.asme.org on 07/02/2019 Terms of Use: http://www.asme.org/about-asme/terms-of-use

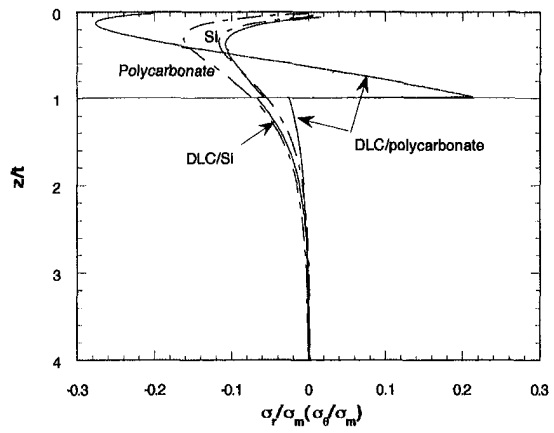

Fig. 17(*a*)

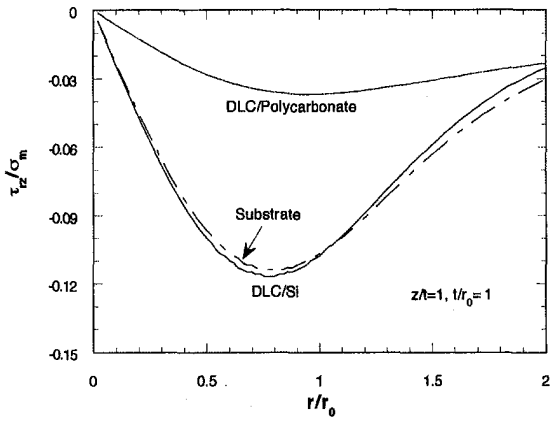

Fig. 17(*b*)

Fig. 17 Stress fields of coating/substrate systems: (a) radial (hoop) stress distribution along the z-axis, and (b) shear stress distribution right above the interface

displacement profile of the coating/substrate system increases as the film thickness increases. The above-stated trend of displacement variation is reversed in the case of hard-coating/soft-substrate systems (Fig. 16). It should be noted that the elastic properties (e.g., Young's modulus) of the thin film can be obtained only approximately using the measurement technique introduced by Oliver and Pethica (1989) when the film thickness is relatively large compared to the indentation loading contact radius, namely, $t \gg r_0$. This is because that the theoretical basis of Ref. 19 is the elastic half-space indentation solution of Harding and Sneddon (1945, 1951). On the other hand, if the indenter penetrates much deeper into the substrate, the elastic modulus of the substrate can be approximated by the saturation value as shown in Fig. 9.

5.3 Failure Mechanisms. The stress field of the coating/substrate system can also be obtained using the technique introduced in section IV. Figure 17 gives the radial (hoop) and shear stress fields for DLC/Si and DLC/polycarbonate systems. The radial and hoop stresses of the coating/substrate systems shown in Fig. 17(*a*) exhibit discontinuities at the interface due to the mismatch of the elastic properties of the film and substrate. In the hard-coating/soft-substrate system (DLC/polycarbonate), the tensile radial and hoop stresses reach their maximum in the film near the interface ($z = t$). The normal stress components are essentially compressive in the cases of bulk Si and DLC/Si. On the other hand, in Fig. 17(*b*), the soft-coating/hard-substrate (DLC/Si) combination exhibits the maximum shear stress near the loading contact region ($r \to r_0$), while the hard-coating/soft-substrate (DLC/polycarbonate) systems show much smaller shear stress.

Obviously, the tensile stress concentration in the film is responsible for film cracking, while interfacial shear stress may induce delamination. This analytical result is consistent with the cracking of hard coating observed in the DLC/polycarbonate system (Fig. 12) and delamination in the soft-coating case (DLC/Si) shown in Fig. 11(*b*).

6 Conclusions

(1) Load-indentation depth data have been obtained for silicon, polycarbonate, DLC/Si, and DLC/polycarbonate systems under nanoindentation. The elastic moduli of the coating/substrate systems can be obtained using the method developed by Oliver and Pharr (1992) for bulk materials. Delamination in the DLC/Si (soft coating) system and cracking in the DLC/polycarbonate (hard coating) system have also been observed.

(2) A theoretical model developed by Li and Chou (1997) has been applied to understand the indentation behavior under axisymmetric loading. Comparisons between experimental data and theoretical predictions of the load-indentation depth relation during unloading show good agreement.

(3) Analytical solutions of the coating/substrate systems suggest that the elastic properties of the thin film can be measured only approximately using the method developed by Oliver and Pharr (1992) when the indentation depth is much smaller than the film thickness. The influences of the film thickness on the indentation behavior can be seen in the displacement profiles at the loading surface. The bulk substrate and coating film always give the bounds of the free surface displacement of the film/substrate systems.

(4) The elastic stress field obtained from the analytical solution provides some insight into the failure mechanism of the coating/substrate system. The analytical result of the stress field is consistent with the observations of delaminations in DLC/Si (soft-coating) and cracking in DLC/polycarbonate (hard-coating).

Acknowledgment

This research was supported by the U.S. Army Research Laboratory. We are grateful to Dr. M. R. Fletcher for her interest in this work and to Dr. A. J. Hsieh, who supplied the specimens used in the experiments. Tsu-Wei Chou thanks the Composite Materials Research Collaborative Program of ARL for partial support of this work.

This Research was also sponsored by the Assistant Secretary for Energy Efficiency and Renewable Energy, Office of Transportation Technologies, as part of the High Temperature Materials Laboratory User Program, Oak Ridge National Laboratory, managed by Lockheed Martin Energy Research Corp. for the U.S. Department of Energy under contract number DE-AC05-96OR22464.

References

Chiu, Y. P., and Hartnett, M. J., 1983, "A Numerical Solution for Layered Solid Contact Problems with Application to Bearings," ASME *Journal of Lubrication Technology,* Vol. 105, pp. 585–590.

Doerner, M. F., and Nix, W. D., 1986, "A Method for Interpreting the Data from Depth-Sensing Indentation Instruments," *Journal of Materials Research,* Vol. 1, No. 4, pp. 601–609.

Evans, A. G., and Hutchinson, J. W., 1984, "On the Mechanics of Delamination and Spalling in Compressed Films," *International Journal of Solids and Structures,* Vol. 20, pp. 455–466.

Evans, A. G., Drory, M. D., and Hu, M. S., 1988, "The Cracking and Decohesion of Thin Film," *Journal of Materials Research,* Vol. 3, pp. 1043–1049.

Gao, H., and Wu, T.-W., 1993, "A Note on the Elastic Contact Stifness of a Layered Medium," *Journal of Materials Research,* Vol. 8, pp. 3229–3232.

Harding, J. W., and Sneddon, I. N., 1945, "The Elastic Stresses Produced by the Indentation of the Plane Surface of a Semi-Infinite Elastic Solid by a Rigid Punch," *Proc. Camb. Phil. Soc.* Vol. 41, pp. 16–26.

Jayachandran, R., Boyce, M. C., and Argon, A. S., 1995, "Mechanics of the Indentation Test and Its Use to Assess the Adhesion of Polymeric Coatings,"

Downloaded From: https://materialstechnology.asmedigitalcollection.asme.org on 07/02/2019 Terms of Use: http://www.asme.org/about-asme/terms-of-use

Adhesion Measurement of Films and Coatings, K. L. Mittal, ed., VSP, pp. 189–215.

Komvopoulos, K., Saka, N., and Suh, N. P., 1987, "The Role of Hard Layers in Lubricated and Dry Sliding," ASME *Journal of Tribology,* Vol. 109, pp. 223–231.

Kral, E. R., Komvopoulos, K., and Bogy, D. B., 1995a, "Finite Element Analysis of Repeated Indentation of an Elastic-Plastic Layered Medium by a Rigid Sphere, Part I. Surface Results," ASME *Journal of Applied Mechanics,* Vol. 62, pp. 20–28.

Kral, E. R., Komvopoulos, K., and Bogy, D. B., 1995b, "Finite Element Analysis of Repeated Indentation of an Elastic-Plastic Layered Medium by a Rigid Sphere, Part II. Subsurface Results," ASME *Journal of Applied Mechanics,* Vol. 62, pp. 29–42.

Lardner, T. J., Giovinazzo, R. J., and Ritter, J. E., 1992, "The Effect of High Modulus Single and Double Layer Coatings on Contact Stress," *Philosophical Magazine A,* Vol. 66, pp. 437–455.

Li, J., and Chou, T.-W., 1997, "Elastic Field of a Thin-Film/Substrate System Under Axisymmetric Loading," *International Journal of Solids and Structures,* Vol. 34, pp. 4463–4478.

Marshall, D. B., and Evans, A. G., 1984, "Measurement of Adherence of Residueally Stressed Thin Films by Indentation. I. Mechanics of Interface Delamination," *Journal of Applied Physics,* Vol. 56, pp. 2632–2638.

Mattewson, M. J., 1986, "Adhesion Measurement of Thin Films by Indentation," *Applied Physics Letter,* Vol. 49, pp. 1426–1428.

Oliver, W. C., Hutchings, R., and Pethica, J. B., 1989, "Measurement of Hardness at Indentation Depths as Low as 20 nanometres," *Microindentation Techniques in Material Science and Engineering,* ASTM STP, Vol. 889, pp. 90–108.

Oliver, W. C., and Pethica, J. B., 1989, "Method for Continuous Determination of the Elastic Stiffness of Contact Between Two Bodies," U.S. Patent No. 4,848,141.

Oliver, W. C., and Pharr, G. M., 1992, "An Improved Technique for Determining Hardness and Elastic Modulus Using Load and Displacement Sensing Indentation Experiments," *Journal of Materials Research,* Vol. 7, No. 6, pp. 1564–1583.

O'Sullivan, T. C., and King, R. B., 1988, "Sliding Contact Stress Field Due to a Spherical Indenter on a Layered Elastic Half-Space," ASME *Journal of Tribology,* Vol. 110, pp. 235–240.

Pethica, J. B., and Oliver, W. C., 1989, *MRS Symposium Procceedings,* Vol. 130, 13–23.

Ritter, J. E., Lardner, T. J., Rosenfeld, L., and Lin, M. R., 1989, "Measurement of Adhesion of Thin Polymer Coatings by Indentation," *Journal of Applied Physics,* Vol. 66, No. 8, pp. 3626–3634.

Rossington, C., Evans, A. G., Marshall, D. B. and Khuri-Yakub, B. T., 1984, "Measurement of Adherence of Residueally Stressed Thin Films by Indentation. II. Experiments with ZnO/Si," *Journal of Applied Physics,* Vol. 56, 2639–2644.

Sneddon, I. N., 1951, *Fourier Transforms,* McGraw-Hill, New York.

Stone, D., LaFontaine, W. R., Alexopoulos, P., Wu, T. W. and Li, C.-Y., 1988, "An Investigation of Hardness and Adhesion of Sputter-Deposited Aluminum on Silicon by Utilizing a Continuous Indentation Test," *Journal of Materials Research,* Vol. 3, pp. 141–147.

Van der Zwaag, S., and Field, J. E., 1982, "The Effect of Thin Hard Coatings on the Hertzian Stress Field," *Philosophical Magazine A,* Vol. 46, pp. 133–150.

Van der Zwaag, S., Dear, J. P., and Field, J. E., 1986, "The Effect of Double Layer Coatings of High Modulus on Contact Stresses," *Philosophical Magazine A,* Vol. 53, pp. 101–111.

APPENDIX

Displacement and Stress Fields of the Coating/Substrate System Under an Axisymmetric Loading

According to Li and Chou's paper (1997) the vertical displacement component is given as

$$w_i(\rho, \varsigma) = \frac{1}{\mu_1 t}\int_0^\infty \bar{q}(\xi)\left[\bar{w}_i^*(\eta, \varsigma) + \frac{\bar{w}_i(\eta, \varsigma)}{D(\eta)}\right]J_0(\rho\eta)d\eta \quad \text{(A1)}$$

where

$$\eta = \xi t, \quad \varsigma = z/t, \quad \text{and} \quad \rho = r/t \quad \text{(A2)}$$

and D is given in Eq. (20), and

$$\bar{w}_1^*(\eta, \varsigma) = \frac{1}{8\gamma_0}(\gamma_1 + \varsigma\eta)e^{-\varsigma\eta}, \quad \bar{w}_0^*(\eta, \varsigma) = 0$$

$$\bar{w}_1(\eta, \varsigma) = \frac{1}{8\gamma_0}\{[1 + 4\gamma_0\gamma_2 + \gamma_1\varsigma\eta]e^{-\varsigma\eta} + [(a - b\gamma_1)\gamma_2 + (a\varsigma - b\gamma_1\varsigma + 16b\gamma_0^2)\eta + 4b(\gamma_2 + 2\gamma_0\varsigma)\eta^2 + 4b\varsigma\eta^3]e^{-(2+\varsigma)\eta} - ab(\gamma_1 + \varsigma\eta)e^{-(4+\varsigma)\eta}\}$$
$$+ \frac{1}{4}\{[(a + b\gamma_1) + 2b(4\gamma_0 - \varsigma)\eta + 4b(1 - \varsigma)\eta^2]e^{-(2-\varsigma)\eta} - 2ab(2\gamma_0 - \varsigma\eta)e^{-(4-\varsigma)\eta}\}$$

$$\bar{w}_0(\eta, \varsigma) = \gamma_0\{[c + d\gamma_3 + 2(c - d + d\varsigma)\eta]e^{-\varsigma\eta} + [-ac - bd\gamma_3 + 2bd(1 + \gamma_3 - \varsigma)\eta - 4bd(1 - \varsigma)\eta^2]e^{-(2+\varsigma)\eta}\} \quad \text{(A3)}$$

with a, b given in eq. (19) and

$$\gamma_0 = 1 - \nu_1, \quad \gamma_1 = 3 - 4\nu_1,$$
$$\gamma_2 = 1 - 2\nu_1, \quad \gamma_3 = 3 - 4\nu_0 \quad \text{(A4)}$$

$$c = \frac{\alpha}{\alpha + \gamma_1}, \quad d = \frac{\alpha}{\gamma_3\alpha + 1}. \quad \text{(A5)}$$

The stress components are

$$\sigma_{ri}(\rho, \varsigma) = \frac{1}{t^2}\int_0^\infty \bar{q}(\xi)\left[\bar{\sigma}_{ri}^*(\eta, \varsigma) + \frac{\bar{\sigma}_{ri}(\eta, \varsigma)}{D(\eta)}\right]\eta J_0(\rho\eta)d\eta - \frac{1}{\rho t^2}\int_0^\infty \bar{q}(\xi)\left[\bar{\sigma}_{ri}^*(\eta, \varsigma) + \frac{\bar{\sigma}_{ri}'(\eta, \varsigma)}{D(\eta)}\right]J_1(\rho\eta)d\eta \quad \text{(A6)}$$

$$\sigma_{\theta i}(\rho, \varsigma) = \frac{1}{t^2}\int_0^\infty \bar{q}(\xi)\frac{\bar{\sigma}_{\theta i}(\eta, \varsigma)}{D(\eta)}\eta J_0(\rho\eta)d\eta + \frac{1}{\rho t^2}\int_0^\infty \bar{q}(\xi)\left[\bar{\sigma}_{\theta i}^*(\eta, \varsigma) + \frac{\bar{\sigma}_{\theta i}'(\eta, \varsigma)}{D(\eta)}\right]J_1(\rho\eta)d\eta \quad \text{(A7)}$$

$$\sigma_{zi}(\rho, \varsigma) = \frac{1}{t^2}\int_0^\infty \bar{q}(\xi)\left[\bar{\sigma}_{zi}^*(\eta, \varsigma) + \frac{\bar{\sigma}_{zi}(\eta, \varsigma)}{D(\eta)}\right]\eta J_0(\rho\eta)d\eta \quad \text{(A8)}$$

$$\tau_{rzi}(\rho, \varsigma) = \frac{1}{t^2}\int_0^\infty \bar{q}(\xi)\left[\bar{\tau}_{rzi}^*(\eta, \varsigma) + \frac{\bar{\tau}_{rzi}(\eta, \varsigma)}{D(\eta)}\right]\eta J_1(\rho\eta)d\eta \quad \text{(A9)}$$

where

$$\bar{\sigma}_{r1}^*(\eta, \varsigma) = \tfrac{1}{2}e^{-\varsigma\eta}, \quad \bar{\sigma}_{r0}^*(\eta, \varsigma) = 0$$

$$\bar{\sigma}_{r1}(\eta, \varsigma) = \tfrac{1}{2}\{[-a + 3b + 2b(2 + \varsigma)\eta - 4b(1 - \varsigma)\eta^2]e^{-(2-\varsigma)\eta} - 2ab(1 + \varsigma\eta)e^{-(4-\varsigma)\eta} - (3 - 2\varsigma\eta)e^{-\varsigma\eta} + 2b[2 - (2 + \varsigma)\eta + 2\varsigma\eta^2]e^{-(2+\varsigma)\eta} - abe^{-(4+\varsigma)\eta}\}$$

$$\bar{\sigma}_{r0}(\eta, \varsigma) = -\frac{2\gamma_0}{\alpha}\{[-c + 3d - 2(c - d(2 + \varsigma))\eta]e^{-\varsigma\eta} + [ac - 3bd + 2bd(2 + \varsigma)\eta + 4bd(1 - \varsigma)\eta^2]e^{-(2+\varsigma)\eta}\}$$

Downloaded From: https://materialstechnology.asmedigitalcollection.asme.org on 07/02/2019 Terms of Use: http://www.asme.org/about-asme/terms-of-use

$$\bar{\sigma}'_{r1}(\eta,\varsigma) = \tfrac{1}{2}\{[-a + b\gamma_1 + 2b(2\gamma_2 + \varsigma)\eta - 4b(1-\varsigma)\eta^2]e^{-(2-\varsigma)\eta} - 2ab(\gamma_2 + \varsigma\eta)e^{-(4-\varsigma)\eta} - (\gamma_1 - 2\varsigma\eta)e^{-\varsigma\eta} + 2b[2\gamma_0 - (2\gamma_2 + \varsigma)\eta + 2\varsigma\eta^2]e^{-(2+\varsigma)\eta} - abe^{-(4+\varsigma)\eta}\}$$

$$\bar{\sigma}'_{r0}(\eta,\varsigma) = -\frac{2\gamma_0}{\alpha}\{[-c + d\gamma_3 - 2(c - d(1-\varsigma))\eta]e^{-\varsigma\eta} + [ac - bd\gamma_3 + 2bd(2\gamma_4 + \varsigma)\eta + 4bd(1-\varsigma)\eta^2]e^{-(2+\varsigma)\eta}\} \quad \text{(A10)}$$

with $\gamma_4 = 1 - 2\nu_0$, and

$$\bar{\sigma}^*_{\theta 1}(\eta,\varsigma) = \bar{\sigma}^*_{r1}(\eta,\varsigma), \quad \bar{\sigma}^*_{\theta 0}(\eta,\varsigma) = 0$$

$$\bar{\sigma}_{\theta 1}(\eta,\varsigma) = -2\nu_1[-(1+2\eta)be^{-(2-\varsigma)\eta} + abe^{-(4-\varsigma)\eta} + e^{-\varsigma\eta} - (1-2\eta)be^{-(2+\varsigma)\eta}]$$

$$\bar{\sigma}_{\theta 0}(\eta,\varsigma) = -\frac{8\nu_0\gamma_0 d}{\alpha}[e^{-\varsigma\eta} - (1-2\eta)be^{-(2+\varsigma)\eta}]$$

$$\bar{\sigma}'_{\theta 1}(\eta,\varsigma) = \bar{\sigma}'_{r1}(\eta,\varsigma), \quad \bar{\sigma}'_{\theta 0}(\eta,\varsigma) = \bar{\sigma}'_{r0}(\eta,\varsigma) \quad \text{(A11)}$$

$$\bar{\sigma}^*_{z1}(\eta,\varsigma) = -\bar{\sigma}^*_{r1}(\eta,\varsigma), \quad \bar{\sigma}^*_{z0}(\eta,\varsigma) = 0$$

$$\bar{\sigma}_{z1}(\eta,\varsigma) = \tfrac{1}{2}\{[a + b + 2b(2-\varsigma)\eta + 4b(1-\varsigma)\eta^2]e^{-(2-\varsigma)\eta} - 2ab(1-\varsigma\eta)e^{-(4-\varsigma)\eta} - (1 + 2\varsigma\eta)e^{-\varsigma\eta} - 2b[(2-\varsigma)\eta + 2\varsigma\eta^2]e^{-(2+\varsigma)\eta} + abe^{-(4+\varsigma)\eta}\}$$

$$\bar{\sigma}_{z0}(\eta,\varsigma) = \frac{2\gamma_0}{\alpha}\{-[c + d + 2(c - d(1-\varsigma))\eta]e^{-\varsigma\eta} + [ac + bd - 2bd(2-\varsigma)\eta + 4bd(1-\varsigma)\eta^2]e^{-(2+\varsigma)\eta}\} \quad \text{(A12)}$$

$$\bar{\tau}^*_{rz1}(\eta,\varsigma) = \bar{\sigma}^*_{z1}(\eta,\varsigma), \quad \bar{\tau}^*_{rz0}(\eta,\varsigma) = 0$$

$$\bar{\tau}_{rz1}(\eta,\varsigma) = \tfrac{1}{2}\{[-a + b + 2b\varsigma\eta - 4b(1-\varsigma)\eta^2]e^{-(2-\varsigma)\eta} - 2ab\varsigma\eta e^{-(4-\varsigma)\eta} + (1 - 2\varsigma\eta)e^{-\varsigma\eta} - 2b(1 - \varsigma\eta + 2\varsigma\eta^2)e^{-(2+\varsigma)\eta} + abe^{-(4+\varsigma)\eta}\}$$

$$\bar{\tau}_{rz0}(\eta,\varsigma) = \frac{2\gamma_0}{\alpha}\{-[c - d + 2(c - d(1-\varsigma))\eta]e^{-\varsigma\eta} + [ac - bd + 2bd\varsigma\eta + 4bd(1-\varsigma)\eta^2]e^{-(2+\varsigma)\eta}\}. \quad \text{(A13)}$$

Downloaded From: https://materialstechnology.asmedigitalcollection.asme.org on 07/02/2019 Terms of Use: http://www.asme.org/about-asme/terms-of-use